

DESIGN OPTIMIZATION, FABRICATION, AND FLOW EXPERIMENT OF 2.5D ROCK-BASED ARTIFICIAL POROUS MEDIA MICROMODEL

Daniel S Park, Saade Bou-Mikael, Sean King, Karsten E Thompson, Clinton S Willson,
Dimitris E. Nikitopoulos
Louisiana State University, USA

ABSTRACT

A rock-based 2.5D artificial porous media micromodel was designed in 13 layers using depth averaging and computational fluid dynamics (CFD), which confirmed accurate in-plane velocity distributions while exhibiting moderate out-of-plane velocity distributions, and provided realistic pore geometry. The rock-based micromodel was microfabricated in polymethylmethacrylate (PMMA) using hot embossing, and used for nanoparticle flow experiment, showing that flow patterns from the PMMA micromodel were similar to those from the designed micromodel. The 2.5D micromodel presented herein will provide insight into factors that are contributing to transport versus retention of the particles.

KEYWORDS

Artificial porous media, 2.5D rock-based micromodel, depth averaging, computational fluid dynamics (CFD), polymethylmethacrylate (PMMA).

INTRODUCTION

Physical micromodels have been widely used to study fluid behaviors in artificial porous media including the effect of surface properties to multiphase transport [1], flow visualization of waterflooding for oil-recovery [2], and water-oil displacement at microscale pores [3]. Most micromodels fabricated by lithography techniques for pore network generation are restricted to 2D patterns with limited out-of-plane velocity distributions. Varying pore depths in a polymer microfluidic micromodel were demonstrated for the study of nanoparticle flow visualization, which enabled the generation of a 2.5D pore network with random bifurcation and recombination geometries and cross-sections [4].

This paper reports design optimization of 2.5D micromodels with varying floor elevation for rock-based artificial porous media using depth averaging and computational fluid dynamics (CFD) from Boise sandstone images to closely represent fluid pathways of real rock samples. The optimized design of the 2.5D micromodel was microfabricated using micromilling of a brass mold insert and hot embossing in polymethylmethacrylate (PMMA). Flow visualization with fluorescent nanoparticles was carried out to compare the flow patterns between the optimized micromodel and the PMMA micromodel.

DESIGN OPTIMIZATION

A core sample of Boise sandstone ($2.5 \times 2.5 \times 3.8 \text{ mm}^3$ section) was scanned by X-ray microtomography, a noninvasive imaging technique, at 5.07 microns/pixel to generate a 3D $500 \times 500 \times 750$ voxel image. A footprint of a $2.03 \times 2.03 \times 2.03 \text{ mm}^3$ section ($400 \times 400 \times 400$ voxel image, $5.07 \mu\text{m}/\text{voxel}$) was extracted to obtain a 3D cut out with multiple stacks of 2D slices (Fig. 1(a)), with permeability of 2 darcys and porosity of 0.2. A subset of slices was used to create a thin section of the image (Fig. 1(b)), which was then processed by depth averaging, projecting the solid voxels to the bottom and moving the void (pore) voxels to the top, which resulted in depth-averaged void structures (Figs. 1(c) and (d)).

Optimization of the depth-averaged structures was carried out by comparing dynamic flow parameters in CFD (velocities and permeability obtained from an in-house Stokes flow simulators) between the original 3-D rock and the depth-averaged micromodels using either the sum of squares error (SSE) for velocities or the absolute fraction error for permeability (Table 1). The distribution for the selected depth average, 23-voxels, showed good agreement in both in-plane velocity distributions (x in the direction of fluid flow and y in the orthogonal direction). Even though the vertical velocity profile in the z-direction did not show good agreement with the true 3D rock structure, it confirmed the velocity generation in the third dimension of the depth-averaged structure. The best permeability match occurred at the 27-voxel depth average.

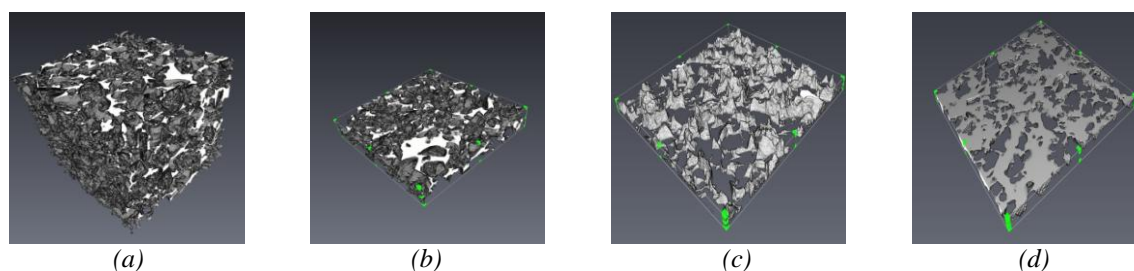


Figure 1. Visualization of the depth averaging process: (a) the extracted image (permeability: 2 darcys, porosity: 0.2) from the X-ray microtomography prior to manipulation, (b) the cut out image prior to depth averaging, and the depth-averaged micromodel from (c) below and (d) above.

Table 1. Summary of velocity distributions and permeability for depth averaged 2.5D micromodels.

Depth		Velocity data			Permeability
No. of voxel	μm	SSE-X	SSE-Y	SSE-Z	Fraction Error
7	35.5	0.2794	0.3122	0.3694	1.000
11	55.8	0.0619	0.0344	0.0990	0.946
15	76.0	0.0132	0.0080	0.0762	0.803
19	96.3	0.0073	0.0055	0.0693	0.642
23	116.6	0.0009	0.0013	0.0635	0.404
27	136.9	0.0046	0.0002	0.0359	0.136
31	157.2	0.0022	0.0015	0.0587	0.247
35	177.5	0.0029	0.0023	0.0568	0.542

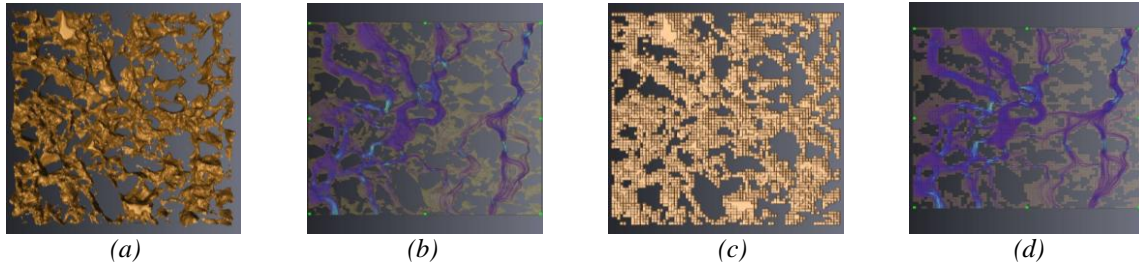


Figure 2. Images of (a) a high-resolution micromodel (permeability: 0.9 darcys, porosity: 0.24) and (b) the corresponding velocity distribution; (c) a low-resolution micromodel (permeability: 1.43 darcys, porosity: 0.2, 13 layers, each layer of 10 μm) and (d) the corresponding velocity distributions (flow direction: bottom to top).

From the comparison of dynamic flow parameters with an emphasis on the in-plane velocity distributions, the optimum design of the 2.5D micromodel at a resolution of 5.07 $\mu\text{m}/\text{pixel}$ was set to 23-voxels (a high-resolution micromodel, Fig. 2(a)) with permeability of 0.9 darcys and porosity of 0.24, and the corresponding velocity profiles were obtained from the Stokes flow simulator (Fig. 2(b)). Due to limitation of our current micromilling system, including a minimum milling bit size of 25 μm and a maximum achievable micromilling aspect ratio of 2, the resolution of the optimized design was lowered by averaging 5x5x2 voxels (or 25x25x10 μm sections) into one unit, and flow simulations were carried out to compare the velocity profiles between the high-resolution micromodel and micromodels with lowered resolution. A final depth of 130 μm (permeability of 1.43 darcys and porosity of 0.2), composed of 13 layers (Fig. 2(c)), showed nearly identical velocity profiles (Fig. 2(d)) to those of the high-resolution micromodel, and selected for microfabrication.

MICROFABRICATION AND FLOW VISUALIZATION

The final low-resolution micromodel was used in AutoCAD to add the inlet and exit regions, pressure measurement ports, and fluidic distribution channels with 13 distinct layers (Figs. 3 (a) and (b)). The low-resolution micromodel design was fabricated by micromilling (KERN MMP-2522, KERN Micro Feinwerktechnik GmbH, Eschenlohe, Germany) of a brass mold insert (Fig. 3(c)) using 25 and 50 μm diameter milling bits, and by hot embossing in 2.5 mm thick PMMA sheets (Fig. 3(d)) using a commercially-available hot embossing machine (HEX02, Jenoptik Mikrotechnik, Jena, Germany). A molding force of ~24 kN was applied to the polymer part for 5 minutes at a mold temperature of 172 $^{\circ}\text{C}$ with a de-molding temperature of 110 $^{\circ}\text{C}$. Scanning electron microscopy (SEM) inspection showed high quality, 13 distinct layers in both the brass mold and the PMMA micromodel. The characterization of the depth profiles was carried out by a non-contact optical profilometer (Nanovea ST400, Micro Photonics Inc., Allentown, PA, USA) and it confirmed the integrity of structural layers with small standard variation (Table 2). The departure from design dimensions was as small as 2.3 μm for the deepest layer. Once cleaning of hot embossed PMMA micromodel devices and generating fluidic through-holes (1 mm diameter) were done, the device was sealed with a thin PMMA sheet (250 μm thick) through thermal fusion bonding (TFB).

After thermal bonding, several 2.5D PMMA micromodels were fitted with inlet and exit port fittings for fluidic interconnects using nanoport assemblies (N-333, Upchurch Scientific, Oak Harbor, CA, USA). The optimized bubble removal protocol [4] was applied to remove bubbles and to fill the PMMA micromodel with water by pulling water from inlet to outlet using a 30 mL syringe for ~30 min and then pushing water from inlet to outlet by the same syringe at 10 $\mu\text{L}/\text{min}$ for ~6 hrs using a syringe pump. Flow visualization were carried out by injecting fluorescent nanoparticles (0.86 μm size, ~4.6 x 10⁸ particles/mL, neutrally buoyant polystyrene particles impregnated with a red fluorescent dye (R900), Duke Scientific Inc., Palo Alto, CA, USA) as tracers at a flow rate of 5 $\mu\text{L}/\text{min}$. Similar flow behavior was observed between the low-resolution micromodel and the PMMA micromodel (Figs. 2(d) and 4).

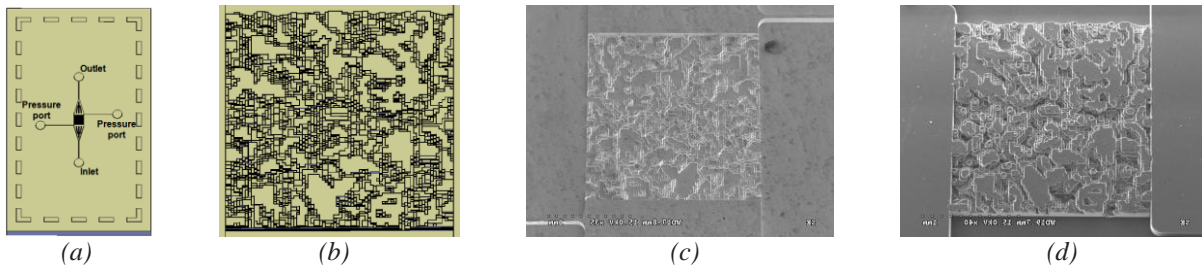


Figure 3. Schematic views of (a) a designed micromodel and (b) close-up of 13 distinct layers; SEM images of (c) a brass mold and (d) a PMMA micromodel.

Table 2. Summary of depth profiles for the fabricated PMMA micromodel.

Layer	Design (μm)	Fabrication (μm)	Layer	Design (μm)	Fabrication (μm)
Layer0	130	132.3 ± 1.5	Layer7	60	58.8 ± 1.2
Layer1	120	118.3 ± 1.2	Layer8	50	50.7 ± 0.7
Layer2	110	110.0 ± 1.7	Layer9	40	39.9 ± 0.3
Layer3	100	99.1 ± 0.4	Layer10	30	30.7 ± 0.3
Layer4	90	90.1 ± 0.8	Layer11	20	21.1 ± 0.3
Layer5	80	80.9 ± 2.5	Layer12	10	10.8 ± 0.7
Layer6	70	69.7 ± 0.4	Layer13	0	0.8 ± 0.8

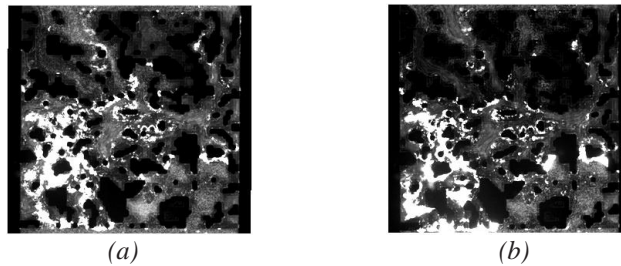


Figure 4. Images of nanoparticle flows at 4X objective lens: (a) 2 min and (b) 40 min after particle injection (flow direction: bottom to top).

CONCLUSIONS

The design of a 2.5D physical micromodel for rock-based artificial porous media was optimized using depth averaging and CFD, and the optimized design of the 2.5D micromodel was microfabricated in PMMA using hot embossing. The PMMA micromodel was used for nanoparticle flow experiment, confirming similar flow patterns between the optimized micromodel and the PMMA micromodel. Further fluidic characterization will allow better understanding of the nanoparticle transport, and ultimately establishing quantitative relationships between observed flow behaviors of nanoparticles to relevant reservoir properties of real porous media materials for oil and gas recovery.

ACKNOWLEDGEMENTS

This work was supported by the Advanced Energy Consortium (AEC, <http://www.beg.utexas.edu/aec/>). We thank J. Guy at the LSU for micromilling of a brass mold insert, the Center for Advanced Microstructures and Devices (CAMD) at LSU for X-ray microtomography and microfabrication support, and Prof. Steven Bryant at the University of Texas in Austin (the Advanced Energy Consortium) for providing a Boise sandstone core sample.

REFERENCES

- [1] V. Berejnov, N. Djilali, and D. Sinton, *Lab-on-chip methodologies for the study of transport in porous media: energy applications*, Lab Chip, 8, pp. 689-693, (2008).
- [2] N.S.K. Gunda, B. Bera, N.K. Karadimitriou, S.K. Mitra, and S.M. Hassanizadeh, *Reservoir-on-a-chip (ROC): a new paradigm in reservoir engineering*, Lab Chip, 11, pp. 3785-3792, (2011).
- [3] M. Wu, F. Xiao, R.M. Johnson-Paben, S. T. Retterer, X. Yin, and K.B. Neeves, *Single- and two-phase flow in microfluidic porous media analogs based on Voronoi tessellation*, Lab Chip, 12, pp. 253-261, (2012).
- [4] D.S. Park, S. King, K.E. Thompson, C.S. Willson, and D.E. Nikitopoulos, *Flow visualization In artificial porous media from microfluidic PMMA devices*, ASME International Mechanical Engineering Congress & Expo, IMECE2011-65266, (2011).

CONTACT

Dimitris E Nikitopoulos 1-225-578-5903 or meniki@me.lsu.edu